Original Article

Coronary artery-to-pulmonary artery fistula in adults: evaluation with 320-row detector computed tomography coronary angiography

Kaibing Hang[1#], Guoli Zhao[1#], Weiwei Su[1], Guangjin Bao[1], Qi Zhao[1], Zizhen Jiao[1], Zhanqi Tian[1], Hui Zhang[1], Lin Nie[1], Rui Luo[1], Lifang Li[1], Min Huang[1], Lijing Shi[2], Shuping Li[1]

[1]Naval Medical Center of People's Liberation Army, Shanghai, China; [2]Department of Radiology, Sixth Medical Center of People's Liberation Army General Hospital, Beijing, China

Contributions: (I) Conception and design: K Hang, G Zhao; (II) Administrative support: L Shi, S Li; (III) Provision of study materials or patients: K Hang, G Bao, Q Zhao, Z Jiao; (IV) Collection and assembly of data: K Hang, H Zhang, L Nie; (V) Data analysis and interpretation: W Su, R Luo, L Li, Z Tian, M Huang; (VI) Manuscript writing: All authors; (VII) Final approval of manuscript: All authors.

[#]These authors contributed equally to this work.

Correspondence to: Lijing Shi. Department of Radiology, Sixth Medical Center of People's Liberation Army General Hospital, No. 6, Fucheng road, Haidian District, Beijing 100048, China. Email: shilijing315@163.com; Shuping Li. Naval Medical Center of People's Liberation Army, No. 338, Huaihai West Road, Changning District, Shanghai 200052, China. Email: lishuping@fudan.edu.cn.

Background: To analyze the imaging features of coronary artery-to-pulmonary artery fistula (CPAF) on coronary computed tomography angiography (CCTA).

Methods: This was a retrospective study of 3,975 patients who underwent 320 row detector CCTA examinations in our hospital from May 2015 to July 2020. A total of 22 patients who diagnosed with CPAF were reviewed for CCTA imaging characteristics, including the origin, number, blood volume, opening size, and course of fistula vessels, and the drainage site, size, and imaging features of the fistula. All cases were analyzed for the presence of coronary atherosclerotic plaque and that of deficient left ventricular myocardial perfusion.

Results: A total of 22 CPAF cases detected by CCTA were collected (men, 11; women, 11; median age, 59.6±10.1 years). There were 7, 10, and 5 cases detected with 1, 2, and 3 fistula vessels, respectively, among which 4 originated from the left coronary artery, 4 from the right coronary artery, and 14 had bilateral origins. There were 10 cases in which the fistula vessels presented as a worm-like tortuous dilation with (n=5) or without (n=5) aneurysm, while 12 cases showed malformed vascular networks with (n=8) or without (n=4) aneurysm, respectively. The calculated incidence of aneurysm formation was 59.09%, and fistula vessels with an aneurysm had larger blood volume than those without. All fistula showed a single drainage site, with an average diameter of 2.81±1.48 mm where the diameter of fistula with aneurysm was larger than that without. The fistula vessels drained into the left anterolateral and anterior walls of main pulmonary artery and the proximal left inferior PA, respectively. Typical jet sign, smoke sign, and isodensity sign were presented in 22, 14 and 1 case, respectively. For the coexistent abnormalities analyzed in 22 cases, 17 participants with CPAF demonstrated hypoperfusion of the fistula vessels, and 11 demonstrated calcified plaque accompanied with luminal stenosis to different degrees.

Conclusions: The 320-row detector CCTA can comprehensively characterize the morphological features of CPAF, which is an optimal choice for physicians to make an accurate assessment before formulating patient management strategies.

Keywords: Coronary artery-to-pulmonary artery fistula (CPAF); 320 row detector X-ray computed tomography; coronary computed tomography angiography (CCTA)

Submitted Jul 14, 2021. Accepted for publication Sep 18, 2021.
doi: 10.21037/atm-21-4404
View this article at: https://dx.doi.org/10.21037/atm-21-4404

© Annals of Translational Medicine. All rights reserved.

Introduction

Coronary artery fistulas (CAFs) are rare vascular abnormalities with an incidence of 0.1–0.2% in adults (1,2), and are characterized by anomalous terminations of the coronary arteries. Coronary artery-to-pulmonary artery fistula (CPAF) is rarer type, accounting for 15–30% of CAFs (3-5). Although the result may give no indication of symptoms at the initial stage of CPAF, the steal phenomenon with diminished myocardial perfusion may occur with disease progression without intervention (6). When the fistula grows large enough to be accompanied by multiple communications or terminations, very tortuous pathways, or even aneurysms formation, surgical intervention is requested (7,8). Herein, an early diagnosis and precise evaluation of CPAF is necessary for eliminating unnecessary patient anxiety and guiding physicians in the establishment of proper management and treatment plans.

Traditional imaging techniques for detecting CPAF mainly include coronary angiography (CAG), transthoracic echocardiography (TTE), and coronary computed tomography angiography (CCTA). The CAG has been seen as a conventional gold standard for diagnosing CPAF (9), but its clinical application is limited by the two-dimensional (2D) imaging modality with significantly diluted contrast, which made it insufficient in visualizing the complex anatomical details (origin, course, termination, and so on) of CPAF. Moreover, the invasive nature of CAG may bring a 0.15% mortality rate and 1.5% morbidity rate (10). The TTE is considered noninvasive and convenient but has failed to accurately display both the coronary artery anatomy of CPAF and the vascular relationships of adjacent structures. The application of CCTA has greatly increased the detectable rate of CAFs (11). By combining the advanced electrocardiogram (ECG)-gated technique with multiple 3D reconstruction modalities, the high-resolution images obtained by CCTA can provide more comprehensive diagnostic information including the exact anatomic description of fistula and complex vascular relationships of adjacent structures, thus becoming a preferred option for diagnosing CCTA in comparison to conventional CAG and TTE.

As mentioned above, an exact and comprehensive understanding of the imaging features of CPAF on CCTA will facilitate physicians to make accurate diagnoses and assessments. To the authors' knowledge, most recent studies regarding the CCTA features of CPAF have been case reports (12-15); however, according to the author's knowledge, case reports are possibly the best way to demonstrate the research. The present study retrospectively reviewed the imaging features of CPAF on CCTA of 22 patients, with the aim of strengthening the understanding of CPAF and assisting physicians in the formulation of better management strategies. We present the following article in accordance with the STROBE reporting checklist (available at https://dx.doi.org/10.21037/atm-21-4404).

Methods

Patients

A total of 3,975 patients who underwent CCTA from May 2015 to July 2017 in Naval Medical Center of People's Liberation Army were retrospectively analyzed, and 22 (0.55%) patients with CPAF were finally collected. All procedures performed in this study involving human participants were in accordance with the Declaration of Helsinki (as revised in 2013). The study was approved by institutional ethics board of Naval Medical Center of People's Liberation Army. Individual consent for this retrospective analysis was waived.

Image acquisition and reconstruction

The CCTA examinations were conducted using a 320-row detector CT scanner (Aquilion ONE TSX-301A, Toshiba, Tokyo, Japan). At 60 min prior to the scan, all participants had their heart rate (HR) checked, and those above 75 beats per minute (bpm) were administered oral betaloc (12.5–50 mg, AstraZeneca, Wuxi, Jiangsu, China). All participants underwent respiratory training before scanning and HR monitoring by ECG throughout the whole scan.

According to the 2-phase contrast media injection protocol, participants were pre-embedded with a 20-gauge catheter through an antecubital vein, using a double tube high-pressure syringe (Antmed Co., Ltd., Shenzhen, Guangdong, China). Participants were first intravenously (IV) injected with 60–90 mL contrast medium (Iopamidol Injection 370 mg/mL, Bracco Sine Pharma, Shanghai, China) at a rate of 4–6 mL/s, and then administered 40 mL of saline solution at the same speed. Prospective ECG-triggered CTCA was performed with the scan parameters as follows: tube voltage 120 kV, tube current 50–200 mAs, collimation 320 mm × 0.5 mm; rotation time 350–375 ms; matrix 512×512, thickness 0.5 mm; field of view (FOV) 160 mm. Retrospective ECG-triggered CTCA was performed with the scan parameters as follows: tube voltage 120 kV, tube current 50–200 mAs, collimation 320 mm × 0.5 mm; rotation time 350 ms; matrix 512×512, thickness 1.0 mm;

© Annals of Translational Medicine. All rights reserved.

Table 1 Patient characteristics and image features

Characteristics	Number
Patients	22/3,975 (0.55%)
Male, n (%)	11 (50.00)
Female, n (%)	11 (50.00)
Age, years	36–81 (59.6±10.1)
Origin and amount of CPAF vessels, n (%)	
Bilateral origins	14 (63.64)
Unilateral coronary artery	8 (36.36)
Right coronary artery	4 (18.18)
Left anterior descending artery	4 (18.18)
Course form and blood volume of CPAF vessels, n (%)	
Worm-like tortuous dilatation	10 (45.45)
Coronary artery ectasia	6 (27.3)
Malformed vascular networks	12 (54.55)
Local coronary artery ectasia	8 (36.36)
Aneurysm	14/22 (63.64)
Average blood volume of the fistula vessels, mm^3	1,841.25 [183–8,640]
Aneurysm, mm^3	2,590.5±2,331.9
Without aneurysm, mm^3	759.1±325.3
Features of the drainage site of CPAF	
Left anterolateral, n (%)	19 (86.36)
Anterior wall of the main pulmonary artery, n (%)	2 (9.09)
Proximal left inferior pulmonary artery, n (%)	1 (4.55)
Average diameter of the drainage site, mm	2.81±1.48 (1.0–6.2)
Aneurysm, mm	2.99±1.37
Without aneurysm, mm	2.54±1.67
Jet sign, n (%)	22 (100.00)
Smoke sign, n (%)	14 (63.64)
Isodensity sign, n (%)	1 (4.55)
Hypoperfusion, n (%)	17 (77.27)

CPAF, coronary artery-to-pulmonary artery fistula.

FOV 160 mm. During the automatic tracking trigger scanning, the trigger threshold was set as 300 Hu and the region of interest (ROI) was set at 1 cm below the tracheal carina on the slice of descending aortic arch. All cases had the same ECG-pulsing window at about 25–80% of the R-R interval. The scan was craniocaudal ranging from 1 cm below the tracheal carina to 2 cm below the diaphragm.

For image reconstruction, the acquired raw data were transported into the imaging postprocessing workstation of Vital Medical Imaging Software (Minnetonka, Minnesota, USA). Images were interpreted via multiple modalities, including multiplanar reformations (MPR), curved planar reconstruction (CPR), maximum intensity projection (MIP), as well as volume rendering (VR).

The CCTA images were reviewed by 5 radiologists with over 5 years' experience in cardiovascular imaging, and any disagreement during imaging interpretation was resolved via discussion for the final conclusion. The CPAF on CTCA images was reviewed and recorded for the origin, number, blood volume, opening size, and course (worm-like dilation/malformed vascular networks/significant aneurysm formation) of fistula vessels, and the drainage site, size, and imaging features (jet sign, smoke sign, isodensity sign) of the fistula. The blood volume was measured using Vital Medical Imaging Software. Referring to previous research (16-18), the sign of worm-like tortuous dilatation was defined by the presence of severely expanded fistula vessels, with obviously tortuousness and with or without aneurysm formation; jet sign is a jet of contrast medium flowing from the supplying artery to the pulmonary artery (PA); smoke sign was recognized when a fuzzy dense contrast medium discharged from the supplying artery and dispersed over less dense contrast into the PA; isodensity sign was decided by a uniformly distributed density contrast between the drainage artery and PA. The formation of an aneurysm was recognized when the maximum diameter of the vascular fistula was 1.5 times larger than the proximal diameter of the original vessel, and the thickest vascular fistula was measured when there was more than 1 vascular fistula (19). Moreover, information about whether the coronary atherosclerotic plaque was stenotic or not, and myocardial perfusion in the left ventricle was also recorded.

Results

Participant demographics and clinical data

In total of 22 participants (men, 11; women, 11; median age, 59.6±10.1 years, range, 36 to 81 years) were collected, including 13 cases who had undergone prospective scanning and 9 for retrospective scanning, and the incidence of CPAF was 0.55% (22/3,975) by CCTA (*Table 1*). The main complaint was chest pain in 3 (13.64%) participants,

© Annals of Translational Medicine. All rights reserved.

chest stuffiness in 13 (59.09%), and palpitation in 4 (18.18%) participants. Totally, 4 (18.18%) participants had a known history of coronary artery disease or myocardial infarction, and 1 (4.55%) had long-term hypertension. During physical examination, 5 (22.73%) participants showed abnormal ECG changes and were diagnosed with sinus arrhythmia, among whom 4 (18.18%) participants demonstrated pathological t-wave on ECG; and 1 (4.55%) was diagnosed with premature ventricular contraction (PVC), supraventricular premature beat (SVEB), and supraventricular tachycardia (SVT).

CCTA findings

Origin and amount of CPAF vessels

Among these 22 cases of CPAF, 8 (36.36%) cases had fistulas originating from unilateral coronary artery, including 4 (18.18%) from the right coronary artery (RCA) and 4 (18.18%) from the left coronary artery (LCA) (*Table 1*). The other 14 (63.64%) cases had bilateral origins including both RCA and LCA. Each of the 4 cases with fistulas originating from RCA had 1 anonymous vessel stemming from the right conus branch. Among the 4 cases that originated from the LCA, 3 had only 1 abnormal branch, 2 were from the proximal left anterior descending artery (LAD), and the other was from the left circumflex artery (LCX) and had an additional left main bronchial-pulmonary artery fistula. Another case had 2 abnormal branches arising from the proximal LAD. Among the 14 cases with bilateral origins, the fistulas were shown as 1 anonymous vessel in 1 case, 2 anonymous vessels in 8 cases, and 3 anonymous vessels in 4 cases. As for the origins, 6 cases were from both the right and left conus artery, 3 were from both the right conus artery and the second branch of LAD, 1 was from both the right coronary sinus and the proximal LAD, and the remaining 3 cases were from both the proximal RCA and the second branch of LAD, both the proximal RCA and the left conus artery, as well as both the RCA, left main artery (LMA), LAD and the first branch of left conus artery, respectively.

Course form and blood volume of CPAF vessels

In our study, worm-like tortuous dilatation of fistula vessels (*Figures 1,2*) were found in 10 (45.45%) cases, among which 6 showed coronary artery ectasia with a diameter 1.5–2 times larger than that of the original vessels. Malformed vascular networks (*Figures 2,3*) were noted in 12 cases (54.55%), and 8 (36.36%) had local coronary artery ectasia with diameters enlarged by 3–6 times. As a result, the incidence of aneurysm formation of the current CPAF cases was 63.64% (14/22). The calculated average blood volume of the fistula vessels was 1841.25 mm^3 (range 183 to 8,640 mm^3), and the fistula vessels accompanied with aneurysm had significantly increased blood volume compared to those without aneurysm (2,590.5±2,331.9 *vs.* 759.1±325.3, P=0.018) (*Table 1*).

Features of the drainage site of CPAF (amount, size, imaging features)

All the CPAF cases presented only a single drainage site, with 19 (86.36%) into the left anterolateral and 2 (9.09%) into the anterior wall of the main pulmonary artery (MPA), and 1 case (4.55%) had a drainage site on the proximal left inferior pulmonary artery (LIPA). The average diameter of the drainage site was 2.81±1.48 mm (range, 1.0–6.2 mm), which was significantly larger in the fistula vessels with aneurysm than those without (2.99±1.37 *vs.* 2.54±1.67, P=0.499). On the CCTA image, the jet sign was demonstrated in 22 cases (100%) (*Figures 1,3*), smoke sign in 14 (63.64%) (*Figure 1*), and isodensity sign in 1 case (4.55%) (*Figure 1*, *Table 1*).

Comorbidities of another coronary artery disease

All 22 cases of CPAF demonstrated insufficient blood perfusion of the cardiovascular system in various degrees, among which 17 (77.27%) cases with hypoperfusion were directly associated with the fistula vessels. Calcified plaque accompanied with diverse degrees of luminal stenosis of cardiac vessels was found in 11 (50%) cases and was directly involved with CPAF vessels in 10 (45.45%) cases. In addition, 4 (18.18%) cases were detected with a myocardial bridge of CPAF vessels without evident luminal stenosis. There was 1 case which exhibited malformed blood vessels connected to the distal LCX and circumvoluted the left the main bronchus.

Discussion

As an accurate, reliable, noninvasive, and convenient imaging modality, combined with superior spatial resolution and advanced 3D and MPRs, CCTA has displayed a greater advantage in detecting CPAF with high efficiency than conventional CAG and TTE. Some researchers have recommended CT as the first imaging modality choice for radiologic evaluation of CPAF (20). In Zhou's study (21), the incidence of CPAF was 0.19% by CCTA, while Li

© Annals of Translational Medicine. All rights reserved.

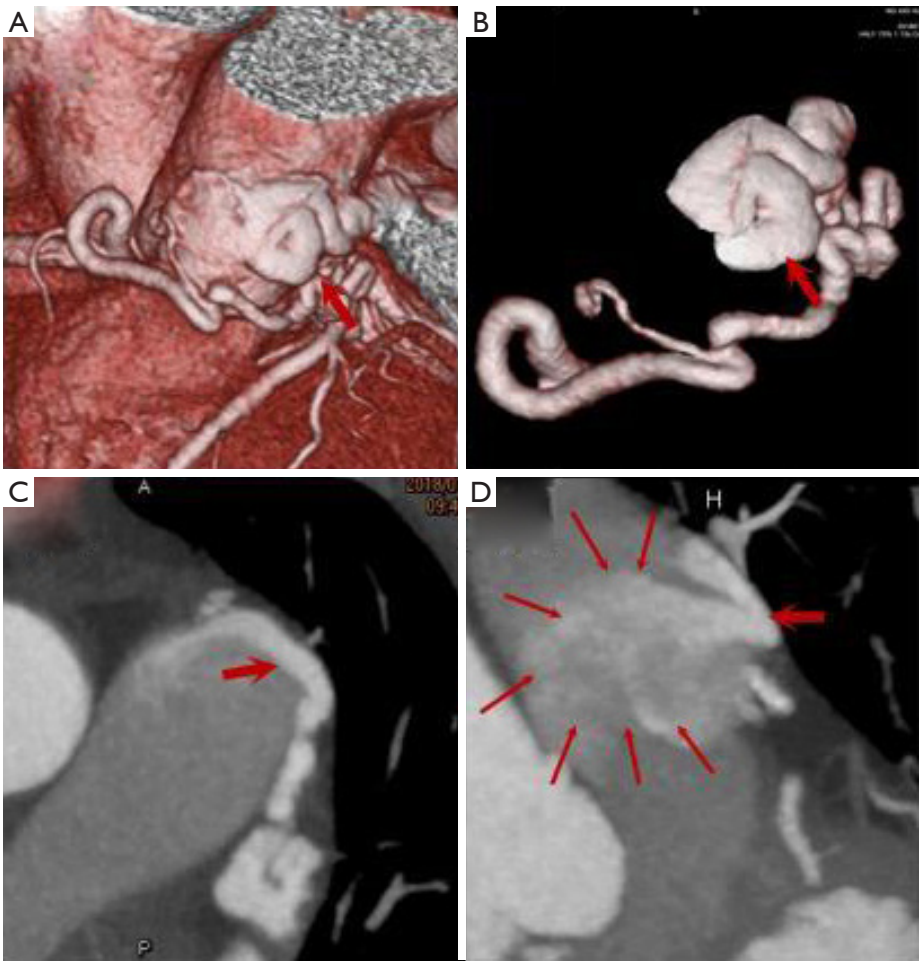

Figure 1 An 81-year-old female with chest distress and pain. VR images (A,B) show worm-like tortuous dilated fistula vessels simultaneously originated from both the RCA and LAD, accompanied with focal aneurysm formation (thick red arrow). CT MPR images on the axial plane (C) a fistula vessel draining into the left lateral wall of MPA (thick red arrow), and MPR image on the coronal plane (D) a huge drainage site with an average diameter of 5.2 mm, and a jet of contrast from supplying artery to MPA forming a typical pierced sign (thick red arrow) and smoke sign (thin red arrow). VR, volume rendering; RCA, right coronary artery; LAD, left anterior descending artery; MPR, multiplanar reconstruction; MPA, main pulmonary artery; CT, computed tomography.

reported a higher incidence of up to 0.36%, in which 20% cases were missed by CAG and 80.9% cases missed by TTE (22). In the present study, the incidence of CPAF detected by CCTA was 0.55%, and the difference compared with previous reports may be caused by the relatively small sample or inclusion criteria of CPAF for CCTA.

Accurately and comprehensively evaluating the imaging features of CPAF on CCTA can provide useful information for formulating a suitable management protocol. According to Li *et al.* (22), CPAF with slight vessel dilation (tubular/simple worm-like tortuous dilation) and without complications (aneurysm/pulmonary artery enlargement/hypertension/myocardial ischemia) requires no follow-up or any treatment; those with significant worm-like tortuous dilation but none of the above complications need follow-up; those with severe worm-like tortuous dilation accompanied with myocardial ischemia should be further evaluated; those with high risk of large aneurysms or associated myocardial ischemia manifestation do need active management. Izumi *et al.* (8) have consistently asserted that when a large fistula of CPAF has high blood flow, multiple communication, an obviously tortuous route, and multiple terminations in the presence of an aneurysm, surgery is essential. Based on the above considerations, this study

© Annals of Translational Medicine. All rights reserved.

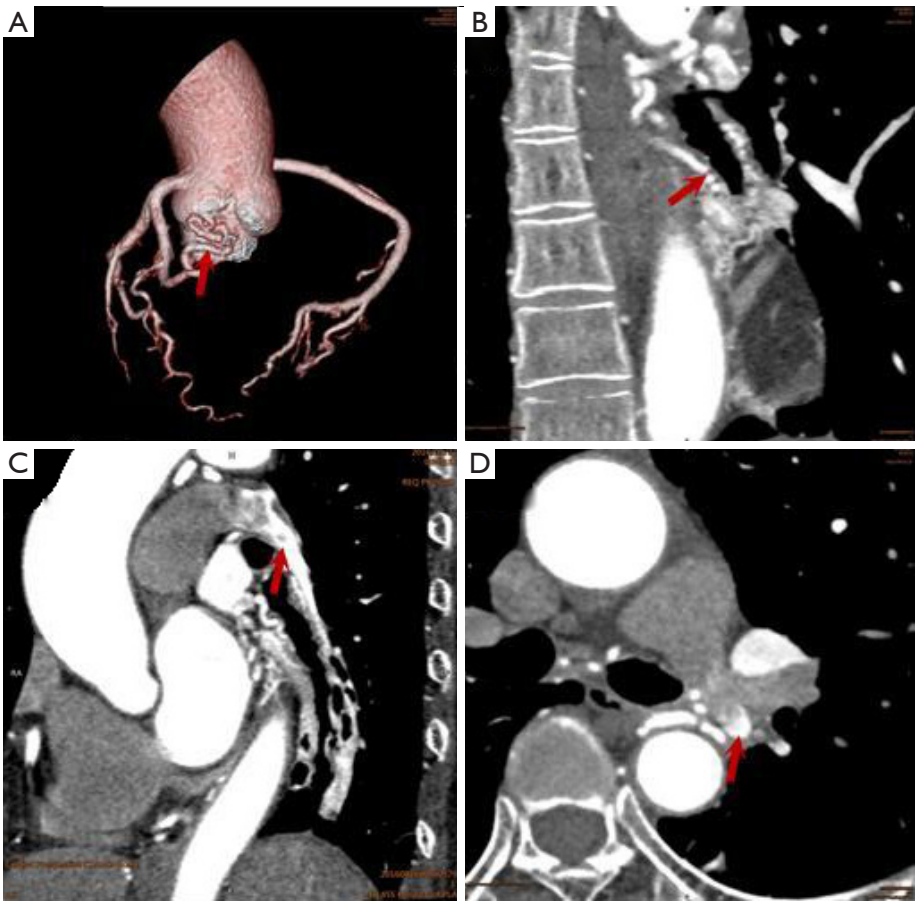

Figure 2 A 61-year-old female with chest distress. VR image (A) worm-like tortuous dilated fistula vessels originated from the LCX (red arrow). CT MPR images on the coronal plane (B) malformed vascular network around the left main bronchus. A small drainage site located at the opening site of the LLPA with an average diameter of 6.2 mm (red arrow) was found on the axial plane (D) of the MPR image, forming a typical isodensity sign on the sagittal plane (C). VR, volume rendering; LCX, left circumflex artery; MPR, multiplanar reconstruction; LLPA, left lower pulmonary artery; CT, computed tomography.

carefully analyzed the imaging characteristics of the 22 cases included in CCTA. In these cases, 68.2% (15/22) cases had multiple (≥2) fistula vessels, which communicated with each other via fistula vessel networks and finally converged into a common drainage site. As for the origin of CPAF, cases with bilateral origins (12, 63.2%) were significantly more common than those with unilateral origins (LAD: 4, 21.1%, RCA: 3, 15.8%). This result was in accordance with studies by Lee *et al.* (17) and Kim *et al.* (23), but contrary to the study by Umaña *et al.* (24). By tracing the path of the fistula vessels, the most common signs were malformed vascular networks with aneurysm formation (8, 36.36%), followed by malformed vascular networks without aneurysm formation (4, 18.18%), and worm-like tortuous dilation. The fistula was dilated to form (6, 27.27%) or not to form (4, 18.18%) aneurysm blood vessels. In total, 63.64% (14/22) of cases formed aneurysm with an increased blood volume which indicated higher hemodynamical shunt flow of the fistula vessels (2,590.5±2,331.9 *vs.* 759.1±325.3 mm^3, P=0.018) and mean diameter of the drainage site (2.99±1.37 *vs.* 2.54±1.67 mm^3, P=0.499) than those without aneurysm formation, all of which supports the idea that aneurysm formation was a considerable indication deserving close follow-up and even surgery due to its potential risk of rupture. The most common drainage site is the left lateral branch of MPA, and the direct imaging manifestations of the drainage site were dominated by the jet sign (22, 100%), followed by the smoke sign (16, 72.73%), and isodensity sign (2, 9.09%). As for the complications, myocardial hypoperfusion was the most common result (19, 100%),

© Annals of Translational Medicine. All rights reserved.

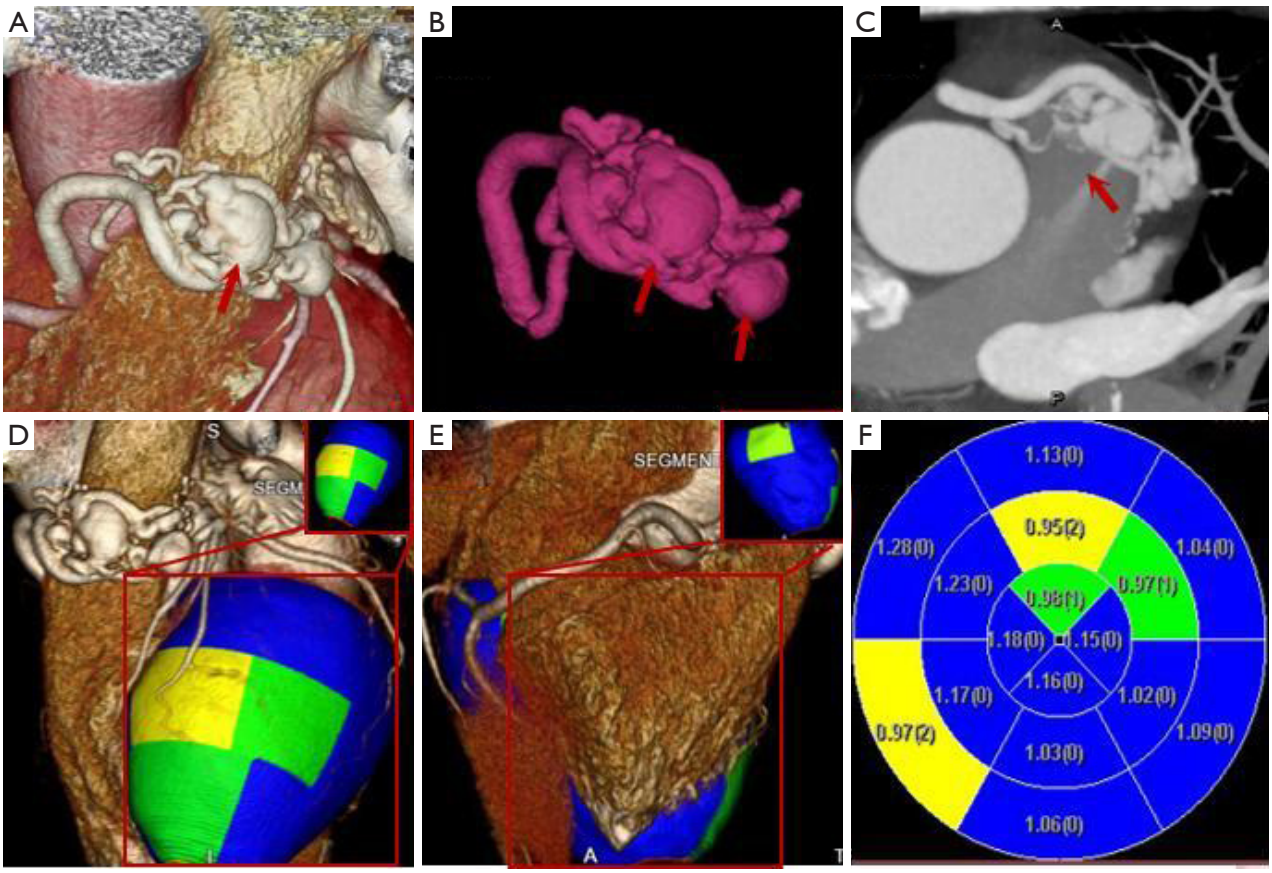

Figure 3 A 55-year-old man with a history of high blood pressure. VR images (A,B) suggested fistula vessels with tumor-like expansion (thick red arrow) which arise from both the RCA and LAD, with multiple branches passing on the surface of the pulmonary artery forming malformed vascular networks. According to the CT MPR image on the axial plane (C), the fistula vessels enter into the MPA from the left anterolateral wall with an averaged diameter of 3.0 mm and form a typical pierced sign (thick red arrow). CTP images (D-F) demonstrate that the TPR value decreased to varying degrees on the segmental of basal posterior (RCA3: TPR =0.97), mid (LAD7: TPR =0.95) anterior, apical anterior (LAD13: TPR =0.98) and mid anterolateral (LCX 12: TPR =0.97) wall of the left ventricle. VR, volume rendering; RCA, right coronary artery; LAD, left anterior descending artery; MPR, multiplanar reconstruction; MPA, main pulmonary artery; CTP, CT perfusion; TPR, transmural perfusion ratio; CT, computed tomography.

most of which (17, 77.27%) were involved with the fistula vessels, and calcified plaque accompanied with luminal stenosis was the second most common symptom. Moreover, myocardial bridge and malformed cardiac vessels was also found in a small portion of cases.

This study had several limitations: First, this was a single-center retrospective study with a small size, and the value of specificity, sensitivity, and diagnostic accuracy of CCTA for diagnosing CPAF was unavailable. Second, the study failed to collect sufficient information about the results of CAG and TTE, and a comparative study with the gold standard was waived. Third, we had planned to conduct a thorough investigation of the relationship of the CT density of CPAF with the diminished myocardial perfusion but this was impeded by the limited data of the case. Future studies will be conducted which will attempt to address these limitations.

Conclusions

The CCTA is highly efficient in detecting and characterizing the anatomic complexity of CPAF, including the origin, number, course, drainage site, and imaging features, as well as the intricate vascular relationships. It is

© Annals of Translational Medicine. All rights reserved.

worthy of consideration as the first choice for screening and diagnosing CPAF.

Acknowledgments

Funding: This work was supported by Internal Research Fund of Naval Medical Center of PLA (18M4701).

Footnote

Reporting Checklist: The authors have completed the STROBE reporting checklist. Available at https://dx.doi.org/10.21037/atm-21-4404

Data Sharing Statement: Available at https://dx.doi.org/10.21037/atm-21-4404

Conflicts of Interest: All authors have completed the ICMJE uniform disclosure form (available at https://dx.doi.org/10.21037/atm-21-4404). The authors have no conflicts of interest to declare.

Ethical Statement: The authors are accountable for all aspects of the work in ensuring that questions related to the accuracy or integrity of any part of the work are appropriately investigated and resolved. All procedures performed in this study involving human participants were in accordance with the Declaration of Helsinki (as revised in 2013). The study was approved by institutional ethics board of Naval Medical Center of People's Liberation Army. Individual consent for this retrospective analysis was waived.

Open Access Statement: This is an Open Access article distributed in accordance with the Creative Commons Attribution-NonCommercial-NoDerivs 4.0 International License (CC BY-NC-ND 4.0), which permits the non-commercial replication and distribution of the article with the strict proviso that no changes or edits are made and the original work is properly cited (including links to both the formal publication through the relevant DOI and the license). See: https://creativecommons.org/licenses/by-nc-nd/4.0/.

References

1. Vavuranakis M, Bush CA, Boudoulas H. Coronary artery fistulas in adults: incidence, angiographic characteristics, natural history. Cathet Cardiovasc Diagn 1995;35:116-20.
2. Yildiz A, Okcun B, Peker T, et al. Prevalence of coronary artery anomalies in 12,457 adult patients who underwent coronary angiography. Clin Cardiol 2010;33:E60-4.
3. Dodge-Khatami A, Mavroudis C, Backer CL. Congenital Heart Surgery Nomenclature and Database Project: anomalies of the coronary arteries. Ann Thorac Surg 2000;69:S270-97.
4. Papadopoulos DP, Perakis A, Votreas V, et al. Bilateral fistulas: a rare cause of chest pain. Case report with literature review. Hellenic J Cardiol 2008;49:111-3.
5. Tomasian A, Lell M, Currier J, et al. Coronary artery to pulmonary artery fistulae with multiple aneurysms: radiological features on dual-source 64-slice CT angiography. Br J Radiol 2008;81:e218-20.
6. Kim SY, Seo JB, Do KH, et al. Coronary artery anomalies: classification and ECG-gated multi-detector row CT findings with angiographic correlation. Radiographics 2006;26:317-33; discussion 333-4.
7. Ishikawa T, Brandt PW. Anomalous origin of the left main coronary artery from the right anterior aortic sinus: angiographic definition of anomalous course. Am J Cardiol 1985;55:770-6.
8. Izumi K, Hisata Y, Hazam S. Surgical repair for a coronary-pulmonary artery fistula with a saccular aneurysm of the coronary artery. Ann Thorac Cardiovasc Surg 2009;15:194-7.
9. Shriki JE, Shinbane JS, Rashid MA, et al. Identifying, characterizing, and classifying congenital anomalies of the coronary arteries. Radiographics 2012;32:453-68.
10. Achenbach S, Ulzheimer S, Baum U, et al. Noninvasive coronary angiography by retrospectively ECG-gated multislice spiral CT. Circulation 2000;102:2823-8.
11. Graidis C, Dimitriadis D, Karasavvidis V, et al. Prevalence and characteristics of coronary artery anomalies in an adult population undergoing multidetector-row computed tomography for the evaluation of coronary artery disease. BMC Cardiovasc Disord 2015;15:112.
12. Chan MS, Chan IY, Fung KH, et al. Demonstration of complex coronary-pulmonary artery fistula by MDCT and correlation with coronary angiography. AJR Am J Roentgenol 2005;184:S28-32.
13. Cay S, Ozbülbül N, Büyükterzi Z, et al. Delineation of a coronary artery to pulmonary artery fistula by multidetector computed tomography angiography. Turk Kardiyol Dern Ars 2008;36:427.
14. Zeina AR, Blinder J, Rosenschein U, et al. Coronary-pulmonary artery fistula diagnosed by multidetector computed tomography. Postgrad Med J 2006;82:e15.

© Annals of Translational Medicine. All rights reserved.

15. Mitsutake R, Miura S, Shiga Y, et al. Coronary-pulmonary artery fistula with anomalous vessels arising from the right coronary sinus detected by 64-MDCT. Intern Med 2009;48:1893-6.
16. Seol SH, Seo GW, Song PS, et al. Coronary-pulmonary artery fistula-multiple diagnostic imaging modalities. J Thorac Dis 2014;6:E27-9.
17. Lee CM, Song SY, Jeon SC, et al. Characteristics of Coronary Artery to Pulmonary Artery Fistula on Coronary Computed Tomography Angiography. J Comput Assist Tomogr 2016;40:398-401.
18. Awasthy N, Radhakrishnan S, Iyer KS, et al. Coronary artery fistula to pulmonary artery: coronary-dependent pulmonary circulation. Ann Thorac Surg 2014;97:716.
19. Lim JJ, Jung JI, Lee BY, et al. Prevalence and types of coronary artery fistulas detected with coronary CT angiography. AJR Am J Roentgenol 2014;203:W237-43.
20. Chandra N, Bastiaenen R, Papadakis M, et al. Sudden cardiac death in young athletes: practical challenges and diagnostic dilemmas. J Am Coll Cardiol 2013;61:1027-40.
21. Zhou K, Kong L, Wang Y, et al. Coronary artery fistula in adults: evaluation with dual-source CT coronary angiography. Br J Radiol 2015;88:20140754.
22. Li JL, Huang L, Zhu W, et al. The evaluation of coronary artery-to-pulmonary artery fistula in adulthood on 256-slice CT coronary angiography: Comparison with coronary catheter angiography and transthoracic echocardiography. J Cardiovasc Comput Tomogr 2019;13:75-80.
23. Kim MS, Jung JI, Chun HJ. Coronary to pulmonary artery fistula: morphologic features at multidetector CT. Int J Cardiovasc Imaging 2010;26:273-80.
24. Umaña E, Massey CV, Painter JA. Myocardial ischemia secondary to a large coronary-pulmonary fistula--a case report. Angiology 2002;53:353-7.

(English Language Editor: J. Jones)

Cite this article as: Hang K, Zhao G, Su W, Bao G, Zhao Q, Jiao Z, Tian Z, Zhang H, Nie L, Luo R, Li L, Huang M, Shi L, Li S. Coronary artery-to-pulmonary artery fistula in adults: evaluation with 320-row detector computed tomography coronary angiography. Ann Transl Med 2021;9(18):1434. doi: 10.21037/atm-21-4404

© Annals of Translational Medicine. All rights reserved.